RESEARCH ARTICLE

Evaluation of Printing Parameters on 3D Extrusion Printing of Pluronic Hydrogels and Machine Learning Guided Parameter Recommendation

Zhouquan Fu[1†], Vincent Angeline[1†], Wei Sun[1,2*]

[1]Department of Mechanical Engineering and Mechanics, Drexel University, Philadelphia, PA 19104, USA
[2]Department of Mechanical Engineering, Tsinghua University, Beijing 100084, People's Republic of China
†*These authors contributed equally to this work*

Abstract: Bioprinting is an emerging technology for the construction of complex three-dimensional (3D) constructs used in various biomedical applications. One of the challenges in this field is the delicate manipulation of material properties and various disparate printing parameters to create structures with high fidelity. Understanding the effects of certain parameters and identifying optimal parameters for creating highly accurate structures are therefore a worthwhile subject to investigate. The objective of this study is to investigate high-impact print parameters on the printing printability and develop a preliminary machine learning model to optimize printing parameters. The results of this study will lead to an exploration of machine learning applications in bioprinting and to an improved understanding between 3D printing parameters and structural printability. Reported results include the effects of rheological property, nozzle gauge, nozzle temperature, path height, and ink composition on the printability of Pluronic F127. The developed Support Vector Machine model generated a process map to assist the selection of optimal printing parameters to yield high quality prints with high probability (>75%). Future work with more generalized machine learning models in bioprinting is also discussed in this article. The finding of this study provides a simple tool to improve printability of extrusion-based bioprinting with minimum experimentations.

Keywords: 3D printing; Bioprinting; Printability; Machine learning; Support vector machine; Pluronic

*Correspondence to: Wei Sun, Department of Mechanical Engineering and Mechanics, Drexel University, Philadelphia, PA 19104, USA; sunwei@drexel.edu

Received: August 19, 2021; **Accepted:** September 3, 2021; **Published Online:** October 15, 2021

Citation: Fu Z, Angeline V, Sun W, 2021, Evaluation of Printing Parameters on 3D Extrusion Printing of Pluronic Hydrogels and Machine Learning Guided Parameter Recommendation. *Int J Bioprint*, 7(4):434. http://doi.org/10.18063/ijb.v7i4.434

1. Introduction

Three-dimensional (3D) bioprinting is a developing technique in the biomedical field for creating a wide range of biological 3D structures, including cell-laden constructs and scaffolds[1]. The bioprinting technique includes several processes, for example, computer-aided design (CAD), 3D printing, and the synthesis of biomaterial and living material[2]. Bioprinting has found widespread applications such as tissue engineering[3,4], reconstructive surgery[5], and drug delivery and screening[6,7]. Bioprinting methods can be generally divided as extrusion, material jetting, and vat polymerization. Vat polymerization utilizes stereolithography or digital light processing to cure polymers of cell-hydrogel suspensions into 3D structures. This method can achieve high resolution but is limited to use with photo responsive bioinks[8]. In ink jetting, droplets of material containing cells are deposited to form printed structures. Variation of droplet sizes and cell concentrations allows for control over concentrations within structures and high resolution. However, low viscosity of the bioinks is often required for the jetting process[9]. Extrusion bioprinting is a bioprinting method derived from traditional thermoplastic 3D printing, incorporating a reservoir and nozzle through which material is extruded layer-by-layer onto a platform. It is unable to reach the resolutions achieved by other methods due to limitations based on nozzle size, but it is low-cost,

versatile, and can be used with bioinks having a much wider range of viscosities[10]. Extrusion bioprinting can be further characterized by two types of printers: pneumatic-based and displacement-based[11]. In a pneumatic-based printer, pressure in the reservoir is manipulated to force material through the nozzle onto the print bed. They allow for precise pressure control which is important to maintaining cell-viability during printing. Motor-based printers utilize a motor to push material down the reservoir and through the nozzle. Despite less precise pressure control, motor-based printers provide better spatial, and flow control and are therefore a better choice when using high viscosity materials[12] such as those in this study.

The overarching type of material used in biofabrication is the bioink. Bioinks are soft materials which contain living cells that are essential for prospective applications[13,14]. A common type of bioink is the hydrogel, which is a highly hydrated cross-linked polymer network capable of providing a tissue-like environment for cells[13,15]. Because of their high hydration and ability to form 3D structures, hydrogels are an ideal candidate for bioprinting which allows cells to survive and grow[13]. Thermo-responsive hydrogels are of interest in 3D bioprinting due to the opportunity to manipulate their properties through temperature control to assist in printing. Among this group of hydrogels is materials such as gelatin, methylcellulose, and PEO-PPO-PEO block copolymers (trade named Pluronic)[11]. Pluronic F127 (PL 127) is of particular interest due to its success for uses as a sacrificial material[3] which can be printed along with other materials then easily removed or washed away leaving other materials intact[11,16].

To characterize outcomes, the term printability is often used. Printability is defined as the geometrical difference between the designed print and the experimental print[15]. Printability is often characterized quantitatively (termed print fidelity[15]) using numerical indices of a print's dimensions and pores[17-19] or qualitatively through visual inspection for tears, breakage, or overall performance. Before testing, printability may also be evaluated on the basis of material properties and performance[15,20]. For this experiment and PL 127's applications in bioprinting, manipulating parameters to create a high-fidelity print is desirable. To simplify and apply experimental results, width index is used as the primary indicator for printability in this experiment. Four parameters were selected for testing based on the hypothesis that they would have a significant impact on the width index and therefore printability of PL 127.

Printing parameters are the wide range of variables which can be adjusted to impact printing outcomes. Printing parameters can be separated into two categories. Process parameters are factors which are set by the printer, such as the height of the nozzle, printing speed, and extrusion speed. Material parameters are related to properties of the material being used, such as its composition, viscosity, and storage or loss modulus. To encompass both types of parameters, nozzle gauge and path height were selected for process parameters, and composition and nozzle temperature were selected for material parameters. Nozzle temperature may be considered as falling under both categories due to thermoresponsive viscosity change of PL 127.

Machine learning (ML) is currently the most rapid developing field and has tremendous potential in 3D printing in terms of developing materials and processes. ML is a tool that establishes statistical models to analyze underling behaviors of a system and give predictions based on training data[21]. There have been several studies trying to fast-track optimal bioprinting parameters and predict printing outcome based on ML algorithms. Conev *et al*. used Random Forest (RF) classifier and regressor to identify suitable printing conditions to recommend for 3D extrusion printing of poly (propylene fumarate). The authors trained the two RF models using a previous factorial design datasets and explored the significance of each parameter based on the feature weights[22]. Menon *et al*. used hierarchical ML (HML) to predict 3D printing of silicone elastomer. A physical modeling layer was integrated in the HML framework, and the model was trained on 38 data points. Previously unseen data were discovered by the HML with high print fidelity and 2.5 times higher printing speed[23]. Ruberu *et al*. employed Bayesian Optimization (BO) to find the optimal printing parameters for 3D extrusion printing of gelatin methacrylate and methacrylated hyaluronic acid composite bioink. The number of experiments required to reach global optima ranged up to 47 with different bioink composition, which was greatly reduced compared with full factorial design (6000 – 10,000)[24]. However, these ML models still require quite large amount of training data points. Considering the cost of biomaterials, living cells, and biofactors, we are looking to adopt an algorithm with a minimal requirement on the number of training data that can still perform well.

The objective of this study is two-fold. The first objective is to evaluate the effects of printing parameters on the printability of PL 127 **(Figure S1)**. The previous research has been conducted on other thermoresponsive hydrogels, including gelatin and alginate[2,17,19,25], or has used pneumatic-based printers which allow for manipulation of pressure which is often studied due to its significant impact on print outcomes[26]. The first study focuses on establishing the understanding of how each parameter affects the outcome of extrusion printing of PL 127. The second objective of this study is to utilize Support Vector Machine (SVM) algorithm to select

sets of optimal printing parameters which have higher (>75%) probability to generate high fidelity PL 127 filaments. Traditional factorial experimental design is time-consuming, and the cost increases exponentially with increasing number of parameters and levels. Building physical models for the bioprinting process are also challenging due to the complex relationship between disparate printing parameters (e.g., biomaterial properties and process parameters) and print outcome. The SVM process optimization methodology was inspired by Aoyagi *et al*[27]. In this study, we selected biomaterial concentration, nozzle temperature, and printing path height as three key parameters. A space-filling Design of Experiment technique was used to select only 12 training data. A 3D process map was generated by the pairwise probability prediction based on SVM model and the validation on the unseen data points showed the model generalized well on the parameter space.

2. Materials and methods

2.1. Preparation of materials

Solutions of PL 127 were prepared by first cooling deionized (DI) water in a 4°C refrigerator, adding Pluronic F-127 (Sigma-Aldrich, St. Louis, MO) powder to create a large 30 w/v% sample, stirring using a magnetic stirrer, and then allowing the sample to homogenize fully in a 4°C refrigerator. Calculations for composition were based on the final solution volume. For lower compositions, the same sample of 30 w/v% PL 127 was then diluted down using DI water, mixed, and again allowed to homogenize fully in a 4°C refrigerator before testing began. This method was used to prevent any false affects appearing in the data due to variations between batches of material.

2.2. Printing and measurement

For all tests, an extrusion-based Bioprinter (BioMaker, SunP Biotech, Cherry Hill, NJ) was used along with the samples synthesized wit PL 127 powder (Sigma-Aldrich, St. Louis, MO). This printer uses motor-based extrusion, as opposed to the also-common pressure-based extrusion used in bioprinting. All CAD designs and slicing are included in the software for this printer, and as such these were the only software used to create and slice a grid design for testing in this experiment. Measurements from microscope images of each print were taken using Fiji/ImageJ.

2.3. Parameter selection for evaluation

Four parameters were selected for testing: two in the material property category and two in the printing parameter category. The material parameters selected were printing temperature and material composition, and process parameters selected were path height and nozzle gauge. Material composition refers to the weight/volume percentage (w/v %) of the PL 127 solution used during testing. This parameter will likely have an effect on print outcomes due to its impact on the viscosity of the material. Nozzle temperature is the temperature that the nozzle and material inside it is held at while printing. It will likely affect prints due to the relation between PL 127 temperature and viscosity. While this parameter is controlled by the printer, its impacts relate to the structure and material properties of PL 127. Therefore, it has been placed under the "material" category of parameter, even though it may be seen as both a "printing" and "material" parameter. Path height is the vertical offset between the printing nozzle and the print bed. During printing the material is stretched by different amounts depending on how high the path height is set. Nozzle gauge refers to the gauge number of the printing nozzle being used. Each nozzle has a different inner and outer diameter.

2.4. Rheological evaluation of PL 127

The viscosities of Pluronic inks were tested by a rheometer (R/S-CPS+, Brookfield, USA). The rheometer is equipped with a temperature control Peltier (0 – 135°C). A P50 plate (radius 25 mm) with 1 mm gap was used in the plate/plate measuring system for all tests. For each test, 2 mL sample was loaded on 4°C plate to fill the gap completely. Viscosities for all concentrations of Pluronic inks were first measured at temperature ramp from 40°C to 4°C for 15 min and constant shear rate at 1/s. The viscosities of all Pluronic inks at 23°C against shear rate ramp were also tested from 0.01 to 100/s for 5 min.

2.5. Variable testing

Baseline values were selected for each variable to be held constant while one category was varied independently. The selected values were a path height of 0.3 mm, nozzle gauge of 25, room temperature (23°C), and a composition of 30% PL 127. Values were varied in one category at a time while all other categories were kept at their baseline values.

2.6. Model grid for printing

The model grid used for printing was designed in the built-in software for the SunP Biotech Bioprinter. The grid was a 0.6 mm tall square with three 0.2 mm layers and a 6 mm side length. Theoretical line width of the infill lines was 0.4 mm.

2.7. Data collection

Before printing, material was pulled from the samples stored in a 4°C refrigerator into a 5 mL syringe. Syringes were allowed to come to room temperature for 10 min

then loaded into the printer for testing. In all temperature tests, the material was given an additional 10 min in the printer to reach the set temperatures before printing. For each combination of parameters, three samples were printed. On each sample, five horizontal line width measurements were taken at random around the grid. Data on vertical lines and pore width were also taken in the same manner. These were taken by imaging the grids under a microscope, then importing the images into Fiji for assessment. Images were converted to 8-bit (black and white) and then sharpened automatically using Fiji's automatic threshold adjustment. After sharpening, the previously mentioned measurements were taken using the line and automatic area selection tools. For each set of parameter tests, data from all three samples were then combined into one larger, 15-item set to calculate the mean and standard deviation.

For a few variables, printing the originally selected grid was not possible due to the effects of the parameters. The 21G nozzle and 20% PL 127 were unable to form a three-layer grid and were instead printed as a one-layer set of lines. In addition, 15% PL 127 was not viscous enough to form any kind of grid and produced no useful data.

2.8. Quantifying prints quality

To characterize prints a line width index was assigned to each print using a method similar to prior research[17]. This allowed for an easy view of how accurate a print was and what kind of error occurred in it. All averaged line values were divided by the theoretical line width, following the formula:

$$\text{Width index} = \frac{\frac{\textit{Experimental Line}}{\textit{Width}}}{\textit{Theoretical}} = \frac{\frac{\textit{Experimental Line}}{\textit{Width}}}{0.4\,mm} \quad (1)$$

2.9. SVM implementation

Uniform Design (UD) technique[28] was used to select 12 experiment data points (**Table 1**) based on a three parameter four level data space $U_{12}(P_3^4)$. Concentration of PL 127 was set at 15, 20, 25, and 30 w/v%. The temperature of the nozzle was selected at 16, 23, 30, and 37°C, and the path height as 0.3, 0.35, 0.4, and 0.45 mm. Twelve data points were normalized before being used as training set.

Table 1. Uniform design with three parameters and four levels

Concentration (Parameter 1)	1	1	1	2	2	2	3	3	3	4	4	4
Temperature (Parameter 2)	4	2	1	3	1	3	4	2	2	1	3	4
Path height (Parameter 3)	4	3	1	3	1	2	2	4	3	2	4	1

A Gaussian kernel was used in the model to transform the feature parameters into high dimensional space so that the nonlinear probability hyperplanes can be constructed. Given m data set $(x^{(i)}, y^{(i)})$, $y^{(i)} = \{-1,1\}$, $i=1,2,\ldots m$, for a certain data sample $x^{(i)}$, the transformation is done by:

$$f_i = exp\left(-\frac{\left\|x^{(i)} - x^{(j)}\right\|^2}{2\sigma^2}\right) \quad (2)$$

so that $x^{(i)}$ is constructed as $(f_1^{(i)}, f_2^{(i)}), f_3^{(i)})$. Here, σ is a scaling parameter and also a hyperparameter to tune in the SVM model. The optimization objective is to maximize the geometric margins of the hyperplane that separates the two classes. The optimization problem is to find the weight w and bias b that minimizes:

$$\min_{w,b,\xi} \frac{1}{2}\|w\|^2 + C\sum_i^m \xi^{(i)} \quad (3)$$

subject to

$$y^{(i)}\left(w^T f^{(i)} + b\right) \geq 1 - \xi^{(i)} \; for\, i = 1\ldots m \quad (4)$$

where ξ is a slack variable and C is the regularization parameter[29].

In this study, an open source SVM software LIBSVM was used on MATLAB to train the model and acquire the parameters w and b[30]. A grid search on two hyperparameters (C and g) was conducted with a threefold cross-validation. C is the regularization parameter applied on the slack variable SVM and g is the gamma parameters in Gaussian kernel ($1/(2\sigma^2)$). The data set is labeled as "1" class (good print) if the calculated width index in method 2.8 is between 0.9 and 1.1, while labeled as "−1" class (bad print) otherwise (**Table 2**). 3D process map was generated based on the pairwise probability estimates on a 3D parameter space[31].

2.10. Statistical analysis

n = 3 prints were made for each parameter test, with n = 5 line measurements taken from each. Mean and standard deviation were measured, and statistical analysis was performed based on original line data. Statistical significance was investigated using data analysis tools within Microsoft Excel. A t-test for two samples assuming equal variances was applied where $P < 0.05$ showed a significant difference between tests. Results displayed in **Figure 2** are of line index data for clarity and insight. A * symbol denotes significance.

Table 2. UD parameter selection and labeling

Concentration w/v %	15	15	15	20	20	20	25	25	25	30	30	30
Temperature (°C)	37	23	16	30	16	30	37	23	23	16	30	37
Path Height (mm)	0.45	0.4	0.3	0.4	0.3	0.35	0.35	0.45	0.4	0.35	0.45	0.3
Label	−1	−1	−1	−1	−1	1	1	−1	−1	1	−1	1

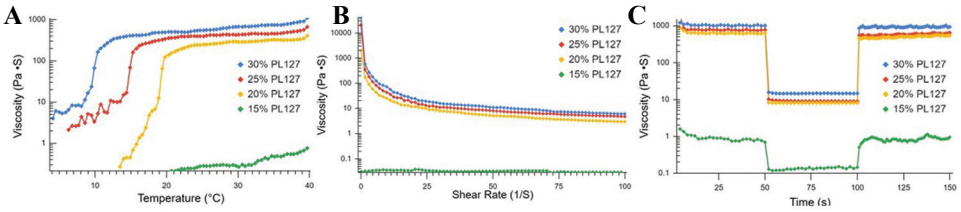

Figure 1. Rheological properties of PL 127 at 30, 25, 20, and 15% concentrations. (A) Temperature sweep of PL 127. Temperature ramp was set from 4 °C to 40 °C over a period of 15 min. (B) Shear rate sweep from 0-100 1/s in 296 s. (C) Thixotropic properties of PL 127 at 23°C. Shear rate stages were set as 0.5/50/0.5 1/s and 50 s for each stage.

3. Results

3.1. Rheological characterization of PL 127

A temperature sweep of the selected concentrations (**Figure 1A**) displayed the differences in viscosity reaction to temperature. Higher concentration resulted in a sharp increase in viscosity at a lower temperature than at lower concentrations. About 30% saw a sharp increase in viscosity at approximately 11°C, 25% at around 15°C, and 20% at around 19°C. Viscosity of 15% concentration was not affected by the temperature change in the same manner and maintained a very low viscosity throughout the temperature sweep process. A decrease in viscosity with respect to increasing shear rate (shear thinning) was observed for all concentrations except 15%, which had no viscosity response to shear rate (**Figure 1B**). PL 127 showed pronounced viscosity recovery for all concentrations (**Figure 1C**). All groups showed prompt decrease in viscosity when the shear rate increased from 0.5 1/s to 50 1/s. Rapid viscosity recovery was also observed when the shear rate decreased back to 0.5 1/s.

3.2. Effects of path height on width index

Path height tests revealed an inverse relationship between path height and line width. A significant difference was found between all tested line widths (0.3, 0.35, and 0.4 mm) (**Figure 2A**). The 0.45 mm test was unable to form a print with cohesive lines for measurement. These tests confirmed the previous hypothesis. Future testing may benefit from expanding intervals at the expense of time and material to find the exact point at which prints begin to fail.

3.3. Effects of nozzle gauge on width index

Nozzle gauge tests revealed no significant difference in line width for all test groups. All tests performed similarly with no significant differences appearing (**Figure 2B**). It is worthwhile to note that due to a difference in stretching effects during printing, 21G tests were only able to form a single layer print. As a result, three-layer tests could not be used to compare the effects of nozzle gauge. Therefore, single layer prints were used for all nozzle gauge tests to accurately determine its effects resulting in line widths below the ideal value for all tests. This is denoted in **Figure 2B** and further considered in the discussion.

3.4. Effects of concentration on width index

Material composition tests yielded results similar to expectations but included more failures than predicted. About 15% tests failed and were unable to form any cohesive structure (**Figure 2C**). The material was not viscous enough to form any type of structure and only bubbled and spread on the print bed. About 20% prints were able to retain some structural integrity but could only produce a single layer print similar to the 21G nozzle. It produced significantly thicker lines than 25% or 30%. A significant difference was not found between 25% and 30%.

3.5. Effects of nozzle temperature on width index

16°C tests produced significantly thicker line widths than all other tests far above the theoretical line width. At above room temperature (23°C, 30°C, and 37°C), all produced similar results which were closer to the theoretical line width (**Figure 2D**). Results of higher temperatures were unexpected given the relationship between PL 127 viscosity and temperature. Higher viscosity was expected to lead to thinner lines, but in these tests, that was not the case. However, 23°C tests did have a higher standard deviation (0.032) than 30 and 37°C tests (0.199 and 0.022, respectively). This indicates that a temperature increase was of use in reducing error in prints and creating more consistent lines.

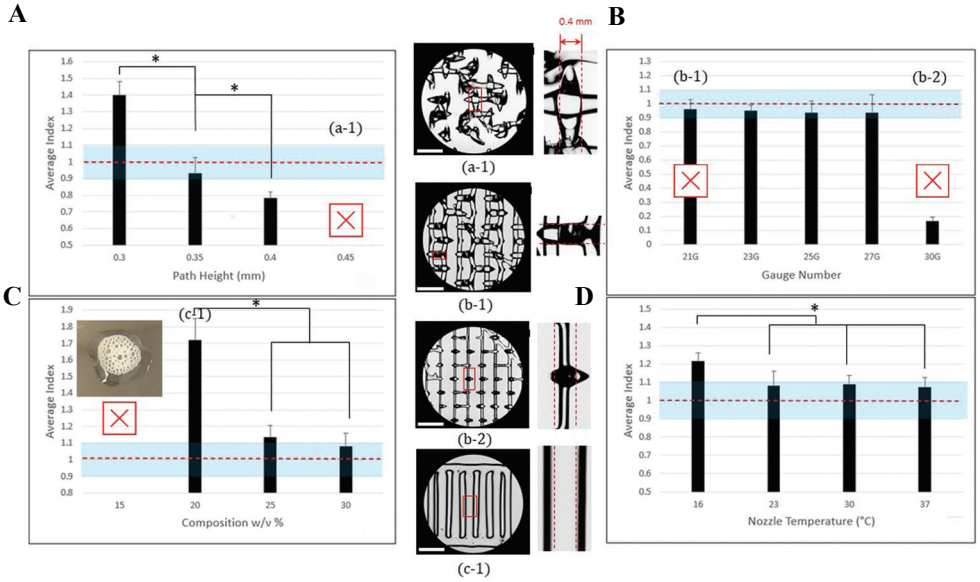

Figure 2. Index representation of parameters. (A) Effects of path height on width index of PL 127 printing. (B) Effects of nozzle gauge. (C) Effects of PL 127 concentration. (D) Effects of nozzle temperature during printing. Horizontal line indicates ideal index value of 1, * denotes statistical significance ($P < 0.05$). Pictures indicate tests which were unable to form the standard three-layer grid. Baseline parameters: 0.3 mm, 25G, 30%, 23°C. Scale bar is 1.87 mm. Distance between two dashed lines is 0.4 mm.

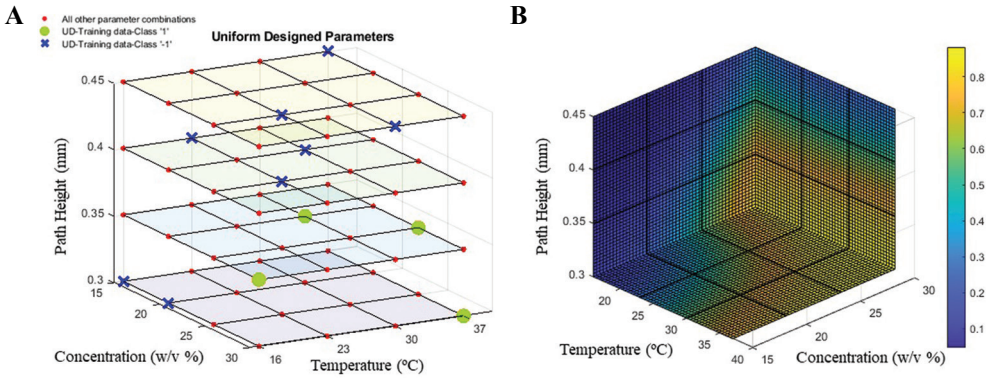

Figure 3. Parameter selection and construction of process map based on SVM prediction. (A) Training data points selection based on UD with three parameters and four levels and 12 tests ($U_{12}(P_3^4)$). (B) 3D process map generated by support vector machine classifier libsvm with regularization parameter $C = 10$ and Gaussian kernel scale parameter $g = 0.1$.

3.6. Parameter selection based on SVM

Training data and its label are shown in **Table 2**. There are totally 12 data points with four good prints and eight bad prints. In the 3D parameter space, all possible combinations of the parameters are labeled in **Figure 3A** which is 4*4*4 = 256 in total. "−1" class data points were labeled in blue cross, "1" class data points were labeled in green circle, and the rest were in red circle. Three-fold cross validation was conducted on the 12 data points and an average 83.3% accuracy score was reached with C taking 10 and g taking 0.1. The generated 3D process map reflects the probability for each data point in the parameter space (concentration, nozzle temperature, and path height) to be classified as good print (class "1"). The higher the color map value, the higher the probability of data point can yield good print.

4. Discussion

4.1. Effect of printing parameters on width index

A common factor between multiple parameters is their connection with the viscosity of PL 127. Viscosity is defined as the ratio of shear stress to shear rate[12]. PL 127 viscosity is dependent on the formation of micelles, which are a formation of connected individual polymer chains[11]. For micelles to form, the material must have reached a certain concentration (critical micelle concentration) and be above the lower critical solution temperature

(LCST)[32]. Micelle formation generally begins at 18-20 w/v %, which is therefore the lowest concentration at which PL 127 can form a cohesive gel capable of printing[11,32]. If the material is above the lower critical solution temperature, micelles will begin to become insoluble in the solution. As temperature increases, micelles will pack together, increasing viscosity, and forming a gel[32]. The temperature where this transition begins (the LCST) is dependent on concentration, with a higher concentration leading to a lower LCST due to the higher rate of polymer interactions[32]. This is shown in **Figure 1**, where 30% PL 127 has a sharp increase in viscosity at 11°C, whereas 25% and 20% do not have the same increase until 15°C and 19°C, respectively.

An understanding of how each print parameter effects printability is an essential basis to optimizing their effects. Material composition's effects result from the viscosity changes between samples. Adding PL 127 will create more viscous material which can improve structural integrity, prevent spreading on the print bed, and improve structural fidelity. At the lowest, concentration must also be high enough that micelle formation begins, and the material gains enough viscosity at certain temperature to form cohesive lines. However, the material cannot be too viscous, otherwise it will require too much force to be extruded and extrudability could be impeded. Therefore, a balance must be struck to achieve the best print outcome. The standard printing range for PL 127 is 25-40%, and at the lowest 18-20% due to micelle formation requirement[11]. This follows from this experiment's data, where 15% was unable to form a print, 20% was just able to form a print in single lines, and 25 and 30% formed a full print. While the differences between 25% and 30% were not found to be significant, the influence of other parameters could make the choice between them relevant.

Nozzle temperature also affects viscosity because of increased micelle packing and formation in the material. As follows, experimental results showed a significant increase in accuracy from 16°C to all higher temperatures. Because of the relationship between micelle formation, temperature, and material composition, an interaction between temperature and composition could be used to further improve accuracy and differentiate parameters. At higher concentrations, micelle formation begins at a lower temperature due to polymer interactions[32]. This is shown by the temperature sweep in **Figure 1**, where higher concentrations saw a sharp increase in viscosity at a lower temperature than lower concentrations. Therefore, at higher temperatures the difference between 25% and 30% PL 127 may become more apparent as 30% will have begun micelle formation before 25% and have accumulated more micelles and maintained a higher viscosity. Because initial tests were both conducted at room temperature, this discrepancy may not have originally been shown. In **Figure 1**, 25% and 30% viscosity are closer at room temperature than at higher temperatures. This possibility could warrant further experimentation to optimize the interplay between parameters when effects would otherwise have reached their individual limits.

Path height impacts printability and width index due to shearing effects during printing. The red region in **Figure 4A** represents the area of the material which is stretched between the print bed and nozzle during printing. The inner region is put under compressive stress, while the outer region is put under tensile stress. As path height increases the stress in the red region also increases, leading to thinly stretched prints and breakage (**Figure 4C and D**). In addition, higher path heights introduce a higher lag time between material leaving the nozzle and reaching the print bed. This may cause material to not follow the printing path correctly and lead to errors, particularly on sharp corners of prints where

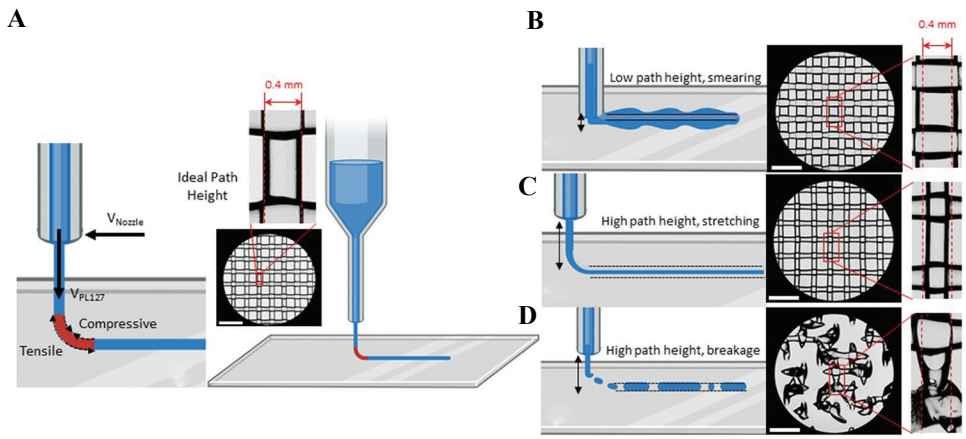

Figure 4. Path height effect representation with experimental examples. (A) Correct path height with stress region highlighted. (B) Low path height leading to interference and smearing. (C) High path height leading to stretching, thin lines. (D) High path height leading to breakage. Correct line width represented by dashed line. Scale bar is 1.87 mm. Created with BioRender.com

material would cut across rather than form a proper corner[25]. Low path heights can have the opposite affect due to the nozzle interfering and spreading the material out into over-deposited thick lines (**Figure 4B**).

Nozzle gauge was not found to have a significant impact on width index, but some other differences were observed between tests. A 21G nozzle corresponds to an inner diameter of 0.58 mm and an outer diameter of 0.81 mm, 23G to an inner/outer diameter of 0.43 and 0.635 mm, 25G to an inner/outer diameter of 0.3 and 0.5 mm, and 27G to an inner/outer diameter of 0.2 and 0.4 mm. It is expected that a change in nozzle diameter will not affect line width as the flow rate out of the nozzle should not be affected if the bioink is considered incompressible. With all other parameters held constant (particularly print speed and extrusion speed) the flow rate out of the nozzle is also constant, and line width therefore cannot change since the same amount of material is being deposited. A difference was noted in the second layer performance of tests. When using wider nozzles, the second layer is stretched more and may tear or fail completely. This can lead to thinner first-layer width as surface tension and the weight of the second layer are absent, leading to less spreading in single-layer prints. 21G tests were unable to form a second layer, 23G tests could form a second layer some errors, and 25G and 27G were able to form a consistent second layer. This problem necessitated single-layer prints for an accurate comparison of how nozzle gauge effects purely line width. However, a complete approach to defining a "best" nozzle gauge would require these problems with certain nozzles be considered.

Effects could be seen if nozzle diameter is small enough to cause a large pressure buildup inside the nozzle tip resulting in a push back on the printer motor. Pressure effects would then impede motor function and extrusion speed would be effectively lowered. To describe this issue a mathematical model of flow rate in the nozzle tip (Eq. 5) can be examined[33]:

$$Q = \left(\frac{n}{3n+1}\right)\pi\gamma_0^{\frac{n-1}{n}}\left(\frac{\partial P/\partial z}{2\eta_0}\right)R^{\frac{3n+1}{n}} \quad (5)$$

where Q represents flow rate, n is the power law index of the fluid, γ is the shear rate, P is pressure, z is the direction in the nozzle axis, η_0 is the limited viscosity, and R is the nozzle radius. If the flow rate (Q) out of the nozzle is to remain constant while the nozzle gauge (R) decreases, then pressure (P) must increase to balance the equation as no other variables will change. In smaller nozzles, this pressure increase could be high enough as to unintentionally lower extrusion speed because of push-back. This is a possible drawback of motor-based printers which is avoided with pressure-based pneumatic printers. To confirm that this effect did not impact testing, a short second experiment was conducted. 21, 23, 25, 27, and 30G nozzles were used with a room temperature sample of 30% PL 127 and extruded for 2 min each **(Figure 2S)**. The amount of material was then weighed and compared, revealing that all nozzles did extrude the same amount of material. Additional testing revealed that effects are seen at nozzle gauges higher than 27G such as 30G (**Figure 2B**).

4.2. Optimal parameter selection based on SVM

We selected two locations on the parameter space; one having higher than 75% probability, the other having lower than 25% probability (**Figure 5**). The scaffold printed with the parameters from low probability region cannot form continuous and stable structure and has a low printability. The printed cube and grid 3D structure were not able to form uniform and accurate shape as desired (**Figure 5A**). While the scaffold printed with the parameter from high printability region was able to generate high printability stable scaffold with multiple test prints having width index evaluated at 0.998 ± 0.049 (mean ± standard deviation). The printed cube and pyramid structure maintained good fidelity and uniformity (**Figure 5B**).

There exists a complex interplay between various printing parameters to achieve desired printability of the scaffold. The impact on the scaffold printability caused by changing one parameter can always be compensated by adjusting another. For example, when printing with a low concentration of PL 127, the low viscosity of the material could be compensated for with a high printing temperature which would increase viscosity. Understanding these relations creates the possibility of any number of "best" parameter combinations which create high fidelity prints. The SVM process optimization method provides a solution to analyze the sophisticated 3D bioprinting black box. Using a minimal preselected training data points can assist construct SVM prediction on a volumetric parameter space so that the optimal printing parameter combinations can be acquired directly without tedious trial and error experiments.

We only used three parameters that were hypothesized to have a significant impact on printability. In fact, a plethora of parameters, such as blend ratio (composite bioink), extrusion pressure (for cell encapsulated printing), and crosslinking strategies (e.g. duration and timing), should also be included. In addition, utilizing governing equations to make more physically informed choice on the parameters is also promising to build a more generalized model.

There were various quantification methods reported on the printability of a scaffold, which significantly affects the generalization of ML model since the label

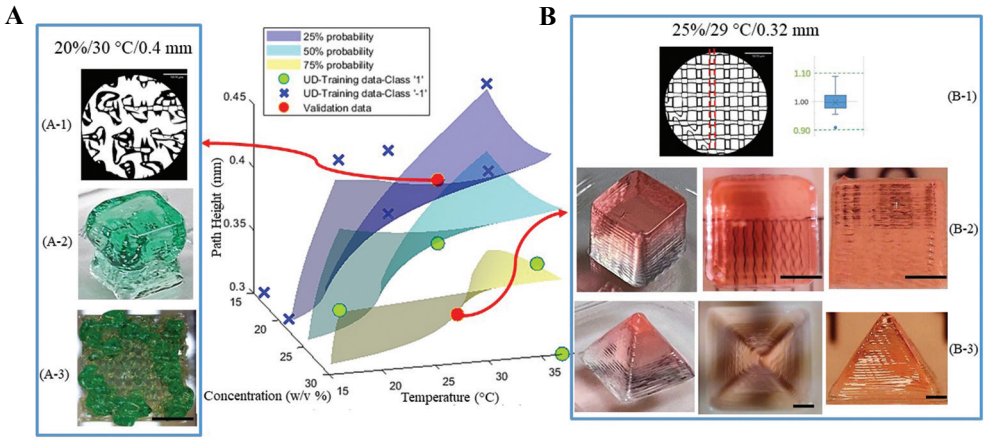

Figure 5. Validation on probability space. Three probability hyperplanes, 25%, 50%, and 75%, were illustrated based on Figure 3B. (A) Validation point selected at 20 w/v% concentration, 30°C nozzle temperature, and 0.4 mm path height. (A-1) Microscopic image evaluating the filament width. (A-2) Printing cube structure (5 × 5 × 5 mm^3). (A-3) Top view of the printed grid structure (5 × 5 × 5 mm^3). (B) Validation point at 25 w/v% concentration, 29°C nozzle temperature, and 0.32 mm path height. (B-1) Microscopic image evaluating the filament width index. (B-2) Printing cube structure (5 × 5 × 5 mm^3) with top view and side view. (B-3) Printing pyramid structure (10 mm × 10 mm × 8 mm) with top and side view. Scale bar for (A-1) and (B-1) is 1.87 mm and 2 mm for the rest.

of a scaffold is a critical information in supervised ML. This problem raises the importance of a standardized metric for printability within the bioprinting community. With a standard evaluation method, ML models could be more generalized and applied across different materials, printers, and applications. This expansion would greatly increase the usefulness of ML in bioprinting and allow for high fidelity prints using new materials without the labor-intensive testing required to continuously build new ML models.

5. Conclusions

In this paper, the effects of path height, nozzle temperature, nozzle gauge, and composition on printability were determined for PL 127 inks. Path height was shown to have an significant impact on printability, while nozzle temperature and composition affect the rheological properties of PL 127, and thus, affect the printability. Nozzle gauge alone was shown to have no effect. Rheological data and an investigation into how these parameters affect printability revealed the importance of viscosity in optimizing parameters and their interactions.

Based on 12 UD training data, a ML model was then built and validated to create a recommendation for optimal combinations of specific printing parameters for extrusion printing of acellular PL 127 bioink. This is our first step and a preliminary study to explore the application of ML toolkit to extrusion-based 3D bioprinting. Future work includes standardizing the quantification of "printability," incorporation of cell viability into the metric (ML labeling), and selection of higher dimensional feature space with more relevant parameters. Building a more generalized ML model creates the continuity between bioprinters and can be used to eliminate the need for mass testing when optimizing the bioprinting of new bioinks.

Acknowledgments

We acknowledge the financial support from SunP Biotech company research grant (Drexel University–260676).

Conflicts of interest

We declaration no conflict of interest.

Author contributions

Z.F. conceptualized the study, wrote the ML section, performed SVM and visualization, reviewed and edited the manuscript. V.A. conducted experiments, wrote the sections related to evaluation printing parameters on print outcome, reviewed and edited the manuscript. W.S. conceptualized the study, reviewed, and edited the manuscript

References

1. Sun W, Starly B, Daly AC, *et al.*, 2020, The Bioprinting Roadmap. *Biofabrication*, 12:022002. http://doi.org/10.1088/1758-5090/ab5158
2. Suntornnond R, Tan EY, An J, *et al.*, 2017, A highly Printable and Biocompatible Hydrogel Composite for Direct Printing of Soft and Perfusable Vasculature-Like Structures. *Sci Rep*, 7:16902. https://doi.org/10.1038/s41598-017-17198-0
3. Kolesky DB, Truby RL, Gladman AS, *et al.*, 2014, 3D

Bioprinting of Vascularized, Heterogeneous Cell-Laden Tissue Constructs. *Adv Mater*, 26:3124–30. https://doi.org/10.1002/adma.201305506

4. An J, Teoh JE, Suntornnond R, *et al.*, 2015, Design and 3D Printing of Scaffolds and Tissues. *Engineering*, 1:261–8. http://doi.org/10.15302/j-eng-2015061
5. Jessop ZM, Al-Sabah A, Gardiner MD, *et al.*, 2017, 3D Bioprinting for Reconstructive Surgery: Principles, Applications and Challenges. *J Plast Reconstr Aesthet Surg*, 70:1155–70. https://doi.org/10.1016/j.bjps.2017.06.001
6. Kondiah PJ, Kondiah PP, Choonara YE, *et al.*, 2020, A 3D Bioprinted Pseudo-Bone Drug Delivery Scaffold for Bone Tissue Engineering. *Pharmaceutics*, 12:166. https://doi.org/10.3390/pharmaceutics12020166
7. Ma X, Liu J, Zhu W, *et al.*, 2018, 3D Bioprinting of Functional Tissue Models for Personalized Drug Screening and *In Vitro* Disease Modeling. *Adv Drug Deliv Rev*, 132:235–51. https://doi.org/10.1016/j.addr.2018.06.011
8. Ng WL, Lee JM, Zhou M, *et al.*, 2020, Vat Polymerization-Based Bioprinting-Process, Materials, Applications and Regulatory Challenges. *Biofabrication*, 12:022001. https://doi.org/10.1088/1758-5090/ab6034
9. Lee JM, Sing SL, Zhou M, *et al.*, 2018, 3D Bioprinting Processes: A Perspective on Classification and Terminology. *Int J Bioprint*, 4:151. https://doi.org/10.18063/ijb.v4i2.151
10. Ouyang L, Yao R, Zhao Y, *et al.*, 2016, Effect of Bioink Properties on Printability and Cell Viability for 3D Bioplotting of Embryonic Stem Cells. *Biofabrication*, 8:035020. https://doi.org/10.1088/1758-5090/8/3/035020
11. Suntornnond R, An J, Chua CK, 2017, Bioprinting of Thermoresponsive Hydrogels for Next Generation Tissue Engineering: A Review. *Macromol Mater Eng*, 302:1600266. https://doi.org/10.1002/mame.201600266
12. Malda J, Visser J, Melchels FP, *et al.*, 2013, 25th Anniversary Article: Engineering Hydrogels for Biofabrication. *Adv Mater*, 25:5011–28. https://doi.org/10.1002/adma.201302042
13. Hospodiuk M, Dey M, Sosnoski D, *et al.*, 2017, The Bioink: A Comprehensive Review on Bioprintable Materials. *Biotechnol Adv*, 35:217–39. https://doi.org/10.1016/j.biotechadv.2016.12.006
14. Gungor-Ozkerim PS, Inci I, Zhang YS, *et al.*, 2018, Bioinks for 3D Bioprinting: An Overview. *Biomater Sci*, 6:915–46. https://doi.org/10.1039/c7bm00765e
15. Fu Z, Naghieh S, Xu C, *et al.*, 2021, Printability in Extrusion Bioprinting. *Biofabrication*, 3:033001. https://doi.org/10.1088/1758-5090/abe7ab
16. Gioffredi E, Boffito M, Calzone S, *et al.*, 2016, Pluronic F127 Hydrogel Characterization and Biofabrication in Cellularized Constructs for Tissue Engineering Applications. *Procedia CIRP*, 49:125–32. https://doi.org/10.1016/j.procir.2015.11.001
17. Kang KH, Hockaday LA, Butcher JT, 2013, Quantitative Optimization of Solid Freeform Deposition of Aqueous Hydrogels. *Biofabrication*, 5:035001. https://doi.org/10.1088/1758-5082/5/3/035001
18. Soltan N, Ning L, Mohabatpour F, *et al.*, 2019, Printability and Cell Viability in Bioprinting Alginate Dialdehyde-Gelatin Scaffolds. *ACS Biomater Sci Eng*, 5:2976–87. https://doi.org/10.1021/acsbiomaterials.9b00167
19. Naghieh S, Sarker MD, Sharma NK, *et al.*, 2019, Printability of 3D Printed Hydrogel Scaffolds: Influence of Hydrogel Composition and Printing Parameters. *Appl Sci*, 10:292. https://doi.org/10.3390/app10010292
20. Paxton N, Smolan W, Bock T, *et al.*, 2017, Proposal to Assess Printability of Bioinks for Extrusion-Based Bioprinting and Evaluation of Rheological Properties Governing Bioprintability. *Biofabrication*, 9:044107. https://doi.org/10.1088/1758-5090/aa8dd8
21. Yu C, Jiang J, 2020, A Perspective on Using Machine Learning in 3D Bioprinting. *Int J Bioprint*, 6:253. http://doi.org/10.18063/ijb.v6i1.253
22. Conev A, Litsa EE, Perez MR, *et al.*, 2020, Machine Learning-Guided Three-Dimensional Printing of Tissue Engineering Scaffolds. *Tissue Eng Part A*, 26:1359–68. https://doi.org/10.1089/ten.tea.2020.0191
23. Menon A, Póczos B, Feinberg AW, *et al.*, 2019, Optimization of Silicone 3D Printing with Hierarchical Machine Learning. *3D Print Addit Manuf*, 6:181–9. https://doi.org/10.1089/3dp.2018.0088
24. Ruberu K, Senadeera M, Rana S, *et al.*, 2021, Coupling Machine Learning with 3D Bioprinting to Fast Track Optimisation of Extrusion Printing. *Appl Mater Today*, 22:100914. https://doi.org/10.1016/j.apmt.2020.100914
25. Holzl K, Lin SM, Tytgat L, *et al.*, 2016, Bioink Properties Before, during and after 3D Bioprinting. *Biofabrication*, 8:032002. https://doi.org/10.1088/1758-5090/8/3/032002
26. Suntornnond R, Tan EY, An J, *et al.*, 2016, A Mathematical Model on the Resolution of Extrusion Bioprinting for the

Development of New Bioinks. *Materials*, 9:756. https://doi.org/10.3390/ma9090756

27. Aoyagi K, Wang H, Sudo H, *et al.*, 2019, Simple Method to Construct Process Maps for Additive Manufacturing using a Support Vector Machine. *Addit Manuf*, 27:353–62. https://doi.org/10.1016/j.addma.2019.03.013
28. Fang KT, Lin DK, Winker P, *et al.*, 2000, Uniform Design: Theory and Application. *Technometrics*, 42:237–48. https://doi.org/10.1080/00401706.2000.10486045
29. Boser BE, Guyon IM, Vapnik VN, 1992, A Training Algorithm for Optimal Margin Classifiers. In: Proceedings of the Fifth Annual Workshop on Computational Learning Theory, p144–52. https://doi.org/10.1145/130385.130401
30. Chang CC, Lin CJ, 2011, LIBSVM: A Library for Support Vector Machines. *ACM Trans Intell Syst Technol*, 2:1–27. https://doi.org/10.1145/1961189.1961199
31. Wu TF, Lin CJ, Weng RC, 2004, Probability Estimates for Multi-Class Classification by Pairwise Coupling. *J Mach Learn Res*, 5:975–1005. https://doi.org/10.5555/1005332.1016791
32. Matanović MR, Kristl J, Grabnar PA, 2014, Thermoresponsive Polymers: Insights Into Decisive Hydrogel Characteristics, Mechanisms of Gelation, and Promising Biomedical Applications. *Int J Pharm*, 472:262–75. https://doi.org/10.1016/j.ijpharm.2014.06.029
33. Khalil S, Sun W, 2007, Biopolymer Deposition for Freeform Fabrication of Hydrogel Tissue Constructs. *Mater Sci Eng C*, 27:469–78. https://doi.org/10.1016/j.msec.2006.05.023